Electronic Supplementary Material (ESI) for Nanoscale.
This journal is © The Royal Society of Chemistry 2014

Supplementary Information

Highly Graphitized Nitrogen-Doped Porous Carbon Nanopolyhedra Derived from ZIF-8 Nanocrystals as Efficient Electrocatalysts for Oxygen Reduction Reactions

Linjie Zhang,[a,b] Zixue Su,[c] Feilong Jiang,[a] Lingling Yang,[a] Jinjie Qian[a,b] Youfu Zhou,[a] Wenmu Li,[a] and Maochun Hong*[,a]

[a]Key Laboratory of Optoelectronic Materials Chemistry and Physics, Fujian Institute of Research on the Structure of Matter, Chinese Academy of Sciences, Fuzhou, 350002, P. R. China

[b]University of Chinese Academy of Sciences, Beijing, 100049, P. R. China

[c]Department of Materials Science, University of Erlangen-Nuremberg, Martensstr. 7, 91058 Erlangen, Germany

Corresponding Author: hmc@fjirsm.ac.cn (M. Hong)

ORR reactions (Eq. 1–3: multistep two-electron pathway; **Eq. 4:** one-step direct four-electron pathway**)**

$$O_2 + H_2O + 2e^- \rightarrow HO_2^- + OH^- \quad \textbf{(1)}$$

$$HO_2^- + H_2O + 2e^- \rightarrow 3OH^- \quad \textbf{(2)}$$

$$2HO_2^- \leftrightarrow O_2 + 2OH^- \quad \textbf{(3)}$$

$$O_2 + 2H_2O + 4e^- \rightarrow 4OH^- \quad \textbf{(4)}$$

Calculation of electron transfer number (*n*)

RDE plots (J^{-1} vs. $\omega^{-1/2}$), were analyzed according to the Koutecky–Levich (**K–L**) equation expressed as **Eq. 5** to assess the apparent number of electrons transferred during ORR (*n*) at various potentials:[1-3]

$$\frac{1}{|J|} = \frac{1}{|J_L|} + \frac{1}{|J_K|} = \frac{1}{B\sqrt{\omega}} + \frac{1}{|J_K|} \quad \textbf{(5)}$$

$$B = 0.2nFC_0(D_0)^{2/3}\upsilon^{-1/6}$$

In the Koutecky–Levich equation, J, J_L, J_K are the measured current density, the diffusion-limiting current density, and the kinetic-limiting current density, respectively; ω is the rotation speed in rpm, F is the Faraday constant (96,485 C mol^{-1}), D_0 is the diffusion coefficient of oxygen in 0.1 M KOH (1.9×10^{-5} cm^2 s^{-1}), υ is the kinetic viscosity (0.01 cm^2 s^{-1}), and C_0 is the bulk concentration of oxygen (1.2×10^{-6} mol cm^{-3}). 0.2 is a constant when the rotation speed is expressed in rpm. The n can be extracted from the slope of the K–L plot.

The transferred electron number per oxygen molecule (*n*) during ORR can be also calculated from **Eq. 6** based on RRDE measurements,[4-5]

$$n = \frac{4I_D}{I_D + \frac{I_R}{N}} \quad \textbf{(6)}$$

and the H_2O selectivity can be analyzed from the following equation:

$$\text{Selectivity}_{H_2O} = \frac{I_D - \frac{I_R}{N}}{I_D + \frac{I_R}{N}} \times 100 = \frac{n-2}{2} \times 100 \quad \textbf{(7)}$$

where I_D, I_R, and $N = 0.30$ are the disk current, ring current, and collection efficiency of Pt ring obtained by using the one-electron $Fe(CN)_6^{3-/4-}$ redox couple, according to the manufacture's instruction, respectively.

References:

1. A. J. Bard, L. R. Faulkner, *Electrochemical Methods: Fundamental and Applications*, Wiley-VCH, New York, 2001, ch. **9**, 331-367.
2. D. Geng, Y. Chen, Y. Chen, Y. Li, R. Li, X. Sun, S. Ye, S. Knights, *Energy Environ. Sci.*, 2011, **4**, 760-764.
3. H. Li, H. Liu, Z. Jong, W. Qu, D. Geng, X. Sun, H. Wang, Int. *J. Hydrog. Energy*, 2011, **36**, 2258-2265.
4. K.P. Gong, F. Du, Z. H. Xia, M. Durstock, L. M. Dai, *Science*, 2009, **323**, 760-764.
5. L. Yang, S. Jiang, Y. Zhao, L. Zhu, S. Chen, X. Wang, Q. Wu, J. Ma, Y. Ma, Z. Hu, *Angew. Chem. Int. Ed.*, 2011, **50**, 7132-7135.

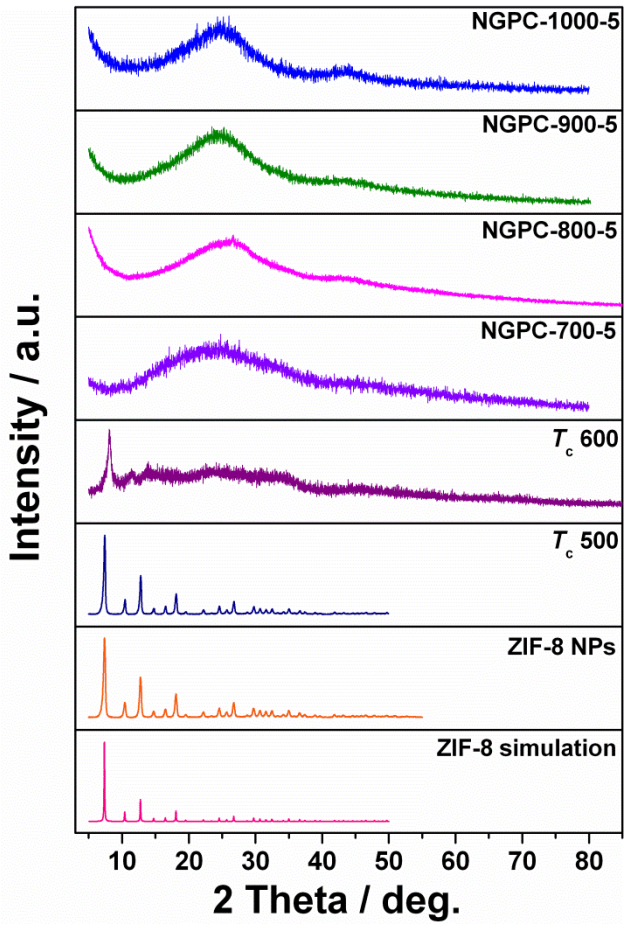

Fig. S1 PXRD diagrams of various pyrolytic products of ZIF-8 nanocrystals at different carbonization temperatures.

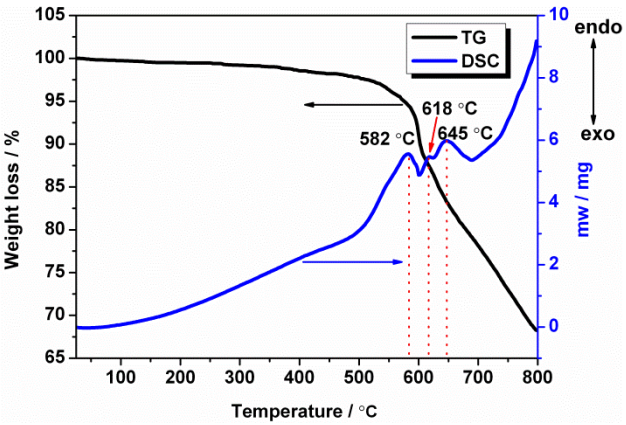

Fig. S2 TGA (black) and DSC (blue) curves of ZIF-8 nanocrystals.

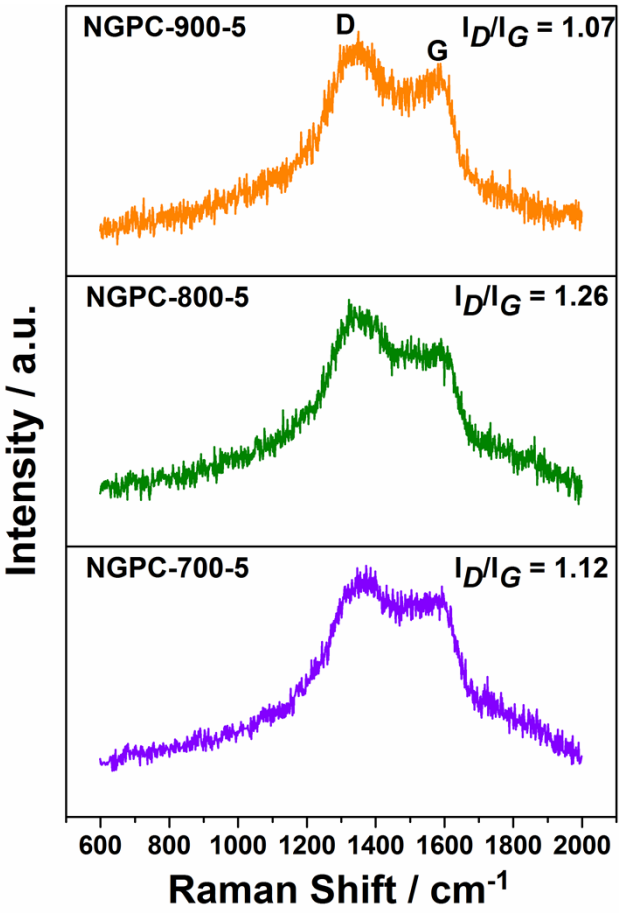

Fig. S3 Raman spectra of NGPCs obtained from 700 to 900 °C.

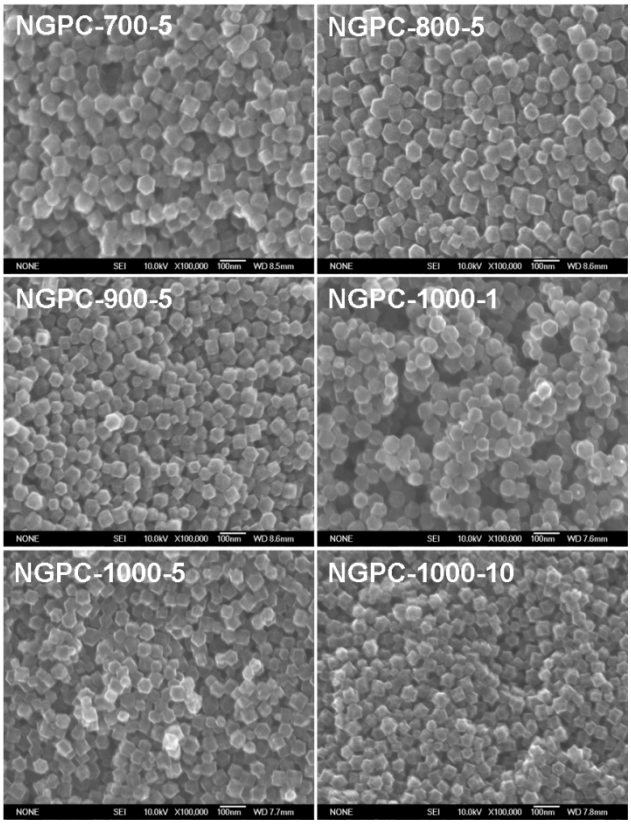

Fig. S4 Representative FE-SEM images of different NGPCs. The particle size decreased gradually as the temperature and carbonization time increased.

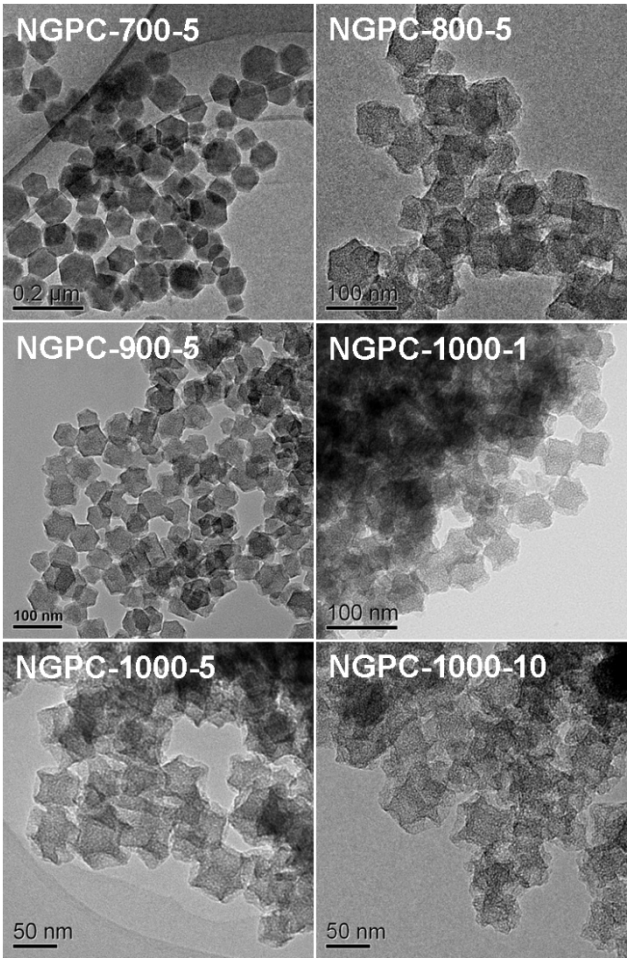

Fig. S5 Representative TEM images of different NGPCs. The surface morphologies of the samples changed from smooth surface to rough surface obviously.

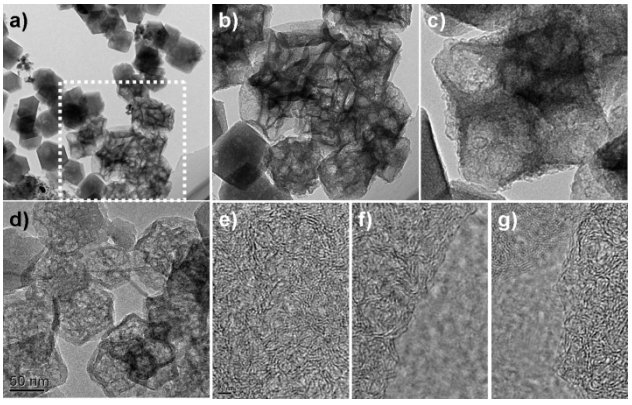

Fig. S6 a) TEM images of NGPCs with cage-like structures; b) and c) enlarged TEM images shown in the rectangular area marked in a); e) to g) HR-TEM images taken from the edges of the particles in a), showing the highly graphitized feature of the NGPCs.

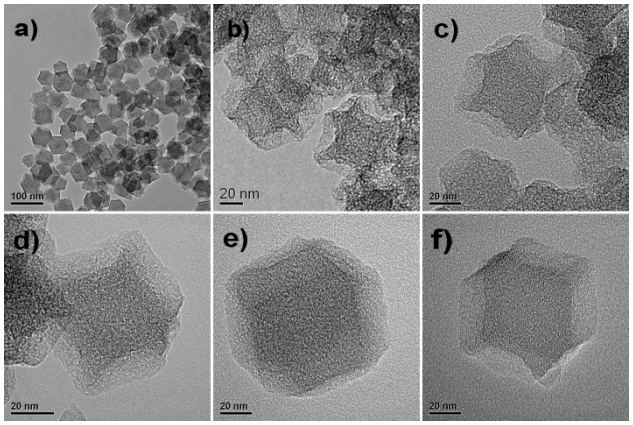

Fig. S7 Typical TEM images of rhombic dodecahedron-like NGPCs with crumpled surfaces.

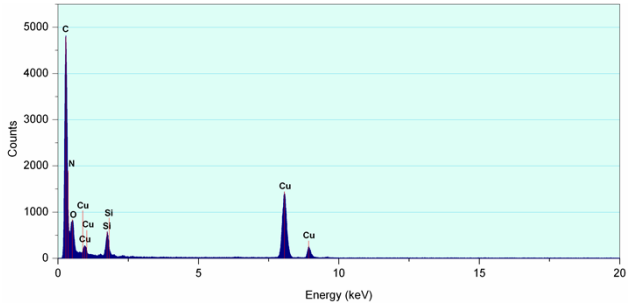

Fig. S8 Typical energy dispersive spectrum (EDS) of NGPC-1000-10.

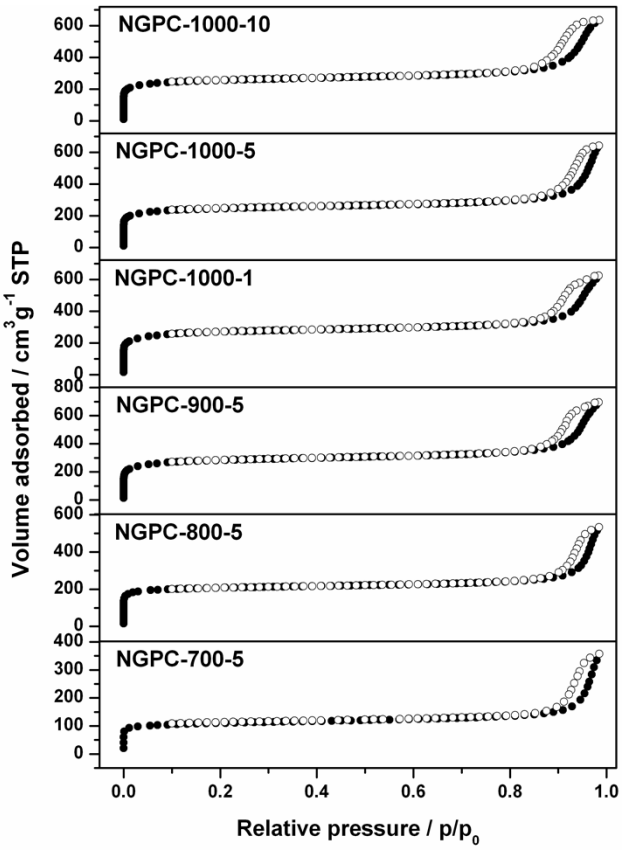

Fig. S9 Nitrogen sorption isotherms (77 K) of NGPCs obtained from different carbonization temperatures and carbonization times.

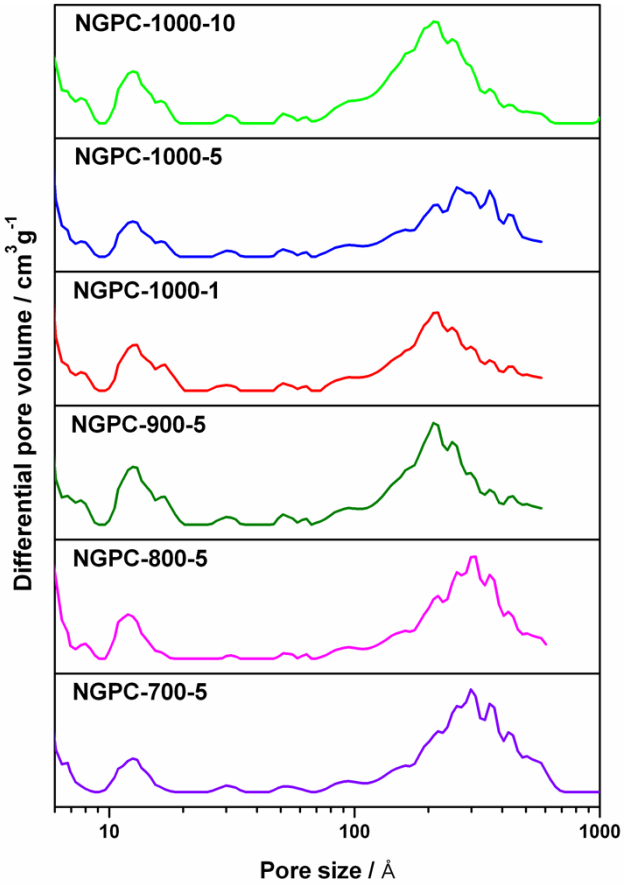

Fig. S10 NL-DFT pore size distributions of NGPCs obtained from different carbonization temperatures and carbonization times.

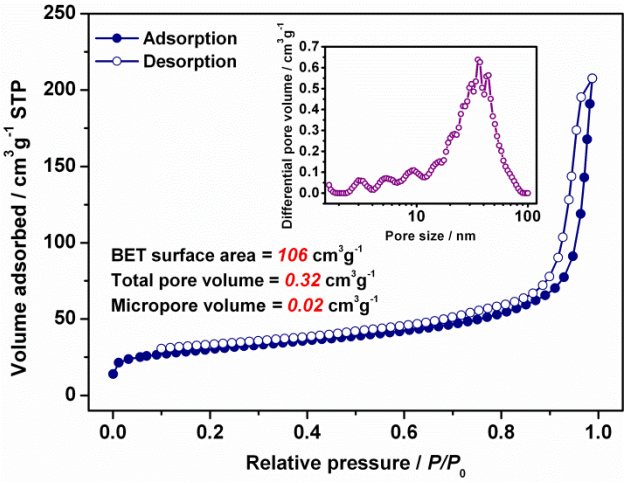

Fig. S11 Nitrogen sorption isotherms (77 K) of NGPC-700-5 sample without acid wash. Inset is the corresponding NL-DFT pore size distribution curve, showing the dominantly meso/macroporosity caused by inter-particle sorption.

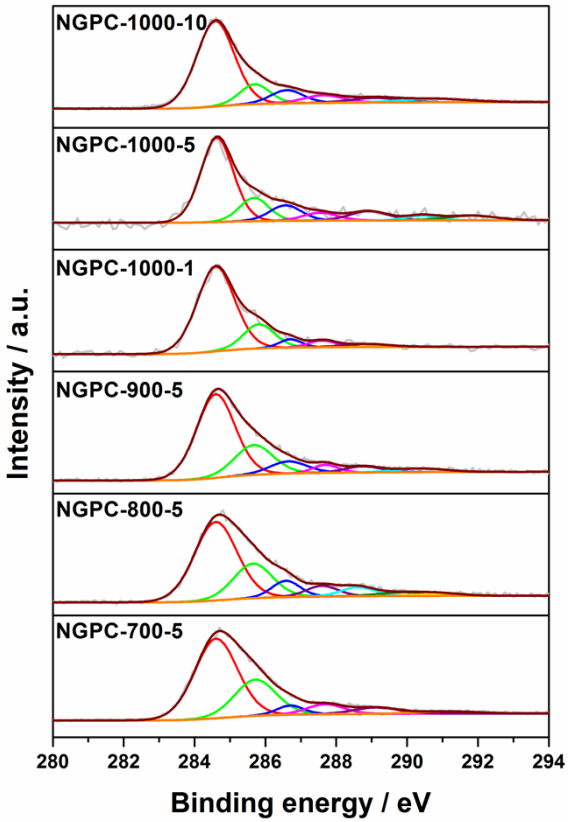

Fig. S12 Deconvoluted C1s spectrum of NGPCs obtained from different carbonization temperatures and carbonization times.

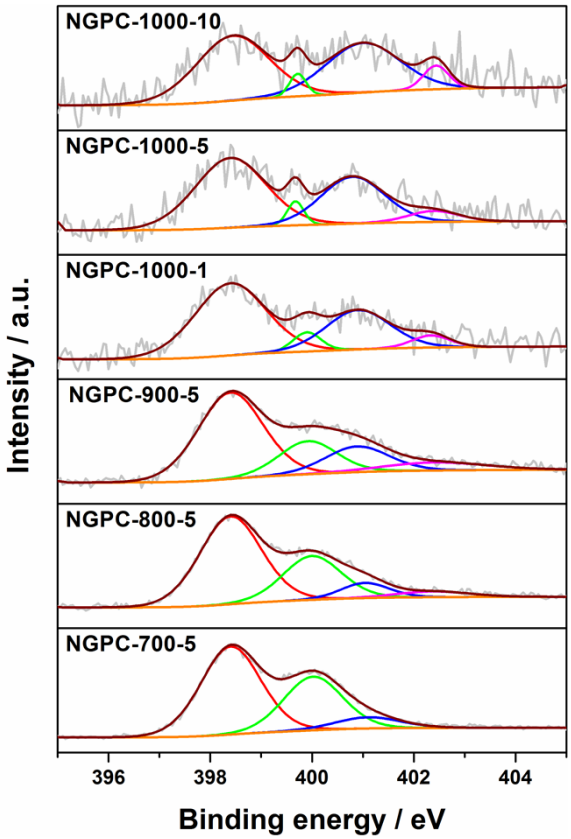

Fig. S13 Deconvoluted N1s spectrum of NGPCs obtained from different carbonization temperatures and carbonization times.

Table S1. C, O, N content and N dopant state of different NGPCs catalysts derived from the XPS analysis.

Sample	C (at.%)	O (at.%)	N (at.%)	Relative content of different N species to total N				$(N1+N3)/N_{total}$
				N1	N2	N3	N4	
NGPC-700-5	68.58	7.52	23.90	0.58	0.35	0.07	N/A	0.65
NGPC-800-5	71.40	7.36	21.24	0.59	0.28	0.09	0.04	0.68
NGPC-900-5	76.26	7.02	16.72	0.57	0.21	0.17	0.05	0.74
NGPC-1000-1	84.62	6.92	8.46	0.61	0.04	0.29	0.06	0.90
NGPC-1000-5	86.90	7.28	5.82	0.58	0.03	0.31	0.08	0.89
NGPC-1000-10	89.33	5.94	4.73	0.46	0.02	0.41	0.11	0.87

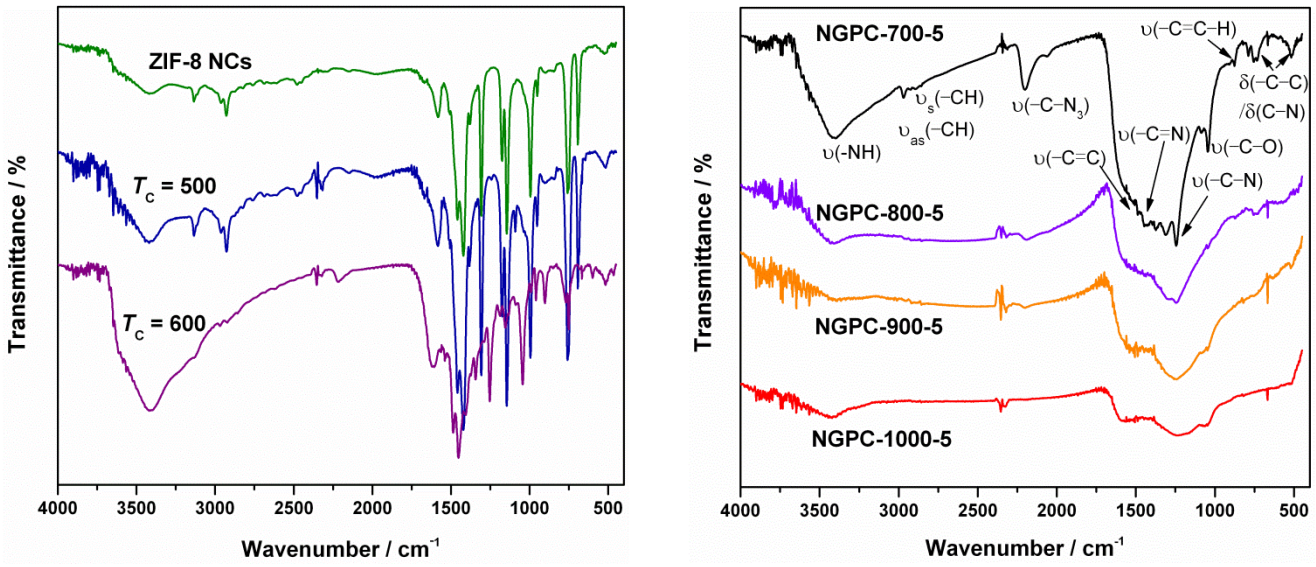

Fig. S14 FT-IR spectra of pyrolytic products of ZIF-8 NCs at different carbonization temperatures.

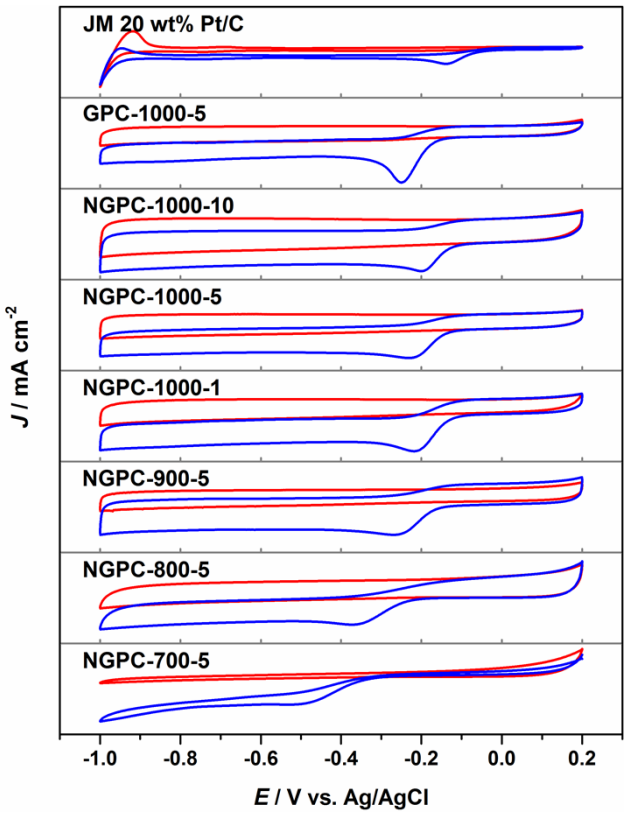

Fig. S15 CV curves of different NGPC samples, GPC-1000-5 and commercial 20 wt.% Pt/C sample (red line, N_2; blue line, O_2) in 0.1 M KOH solution (scan rate: 10 mV s^{-1}).

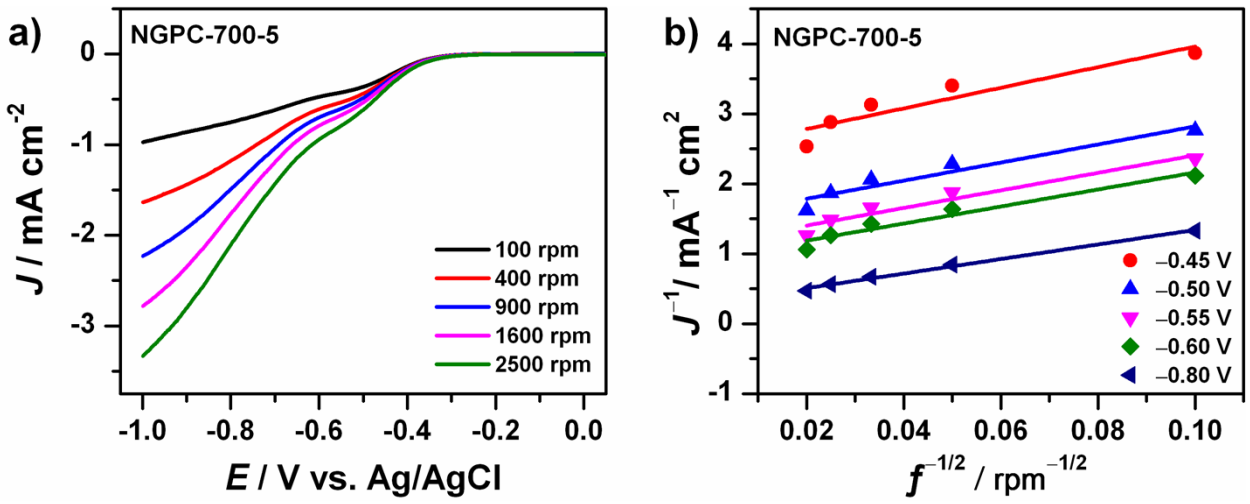

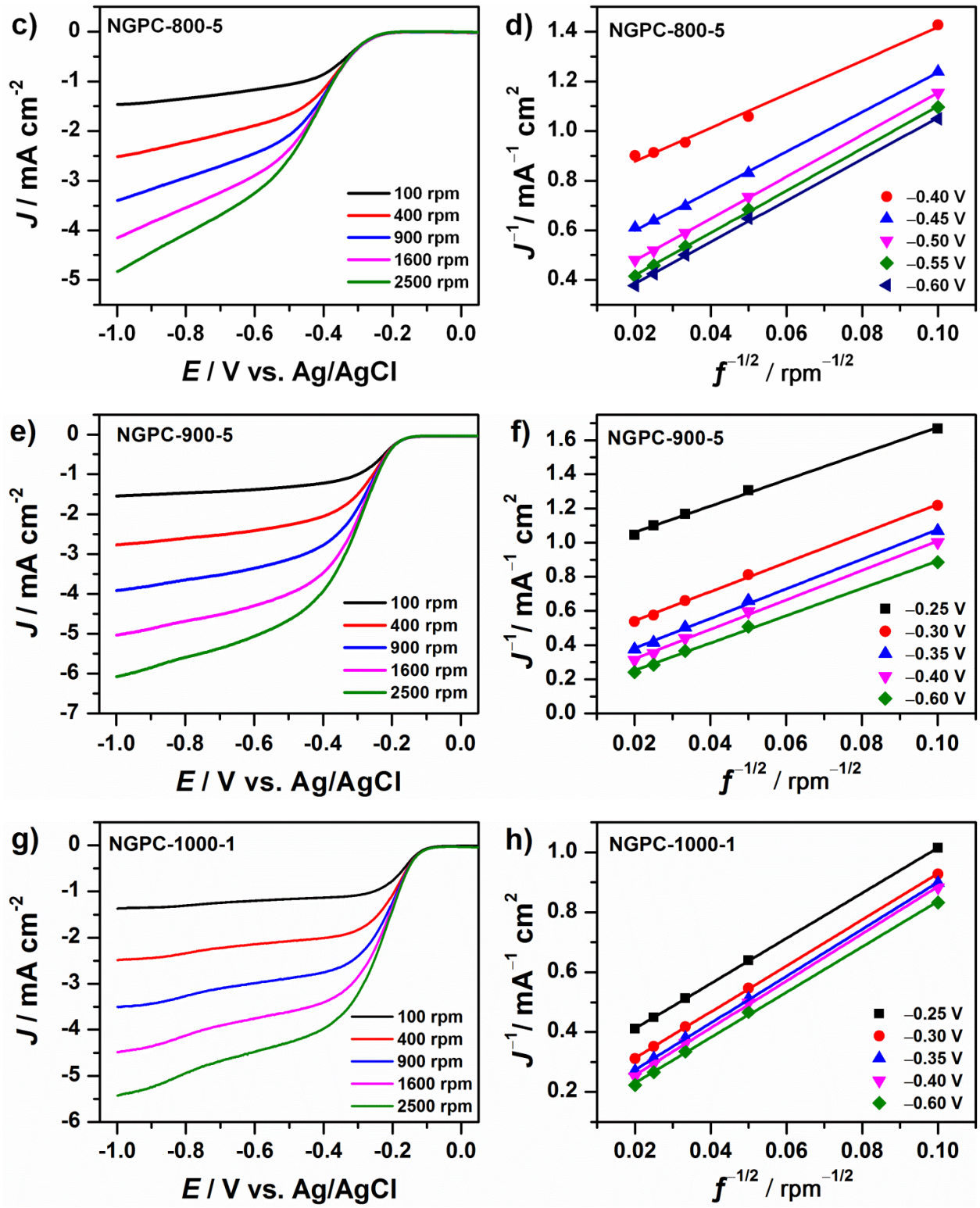
c)
NGPC-800-5
J / mA cm-2
E / V vs. Ag/AgCl
100 rpm
400 rpm
900 rpm
1600 rpm
2500 rpm
d)
NGPC-800-5
J-1/ mA-1 cm2
f-1/2 / rpm-1/2
–0.40 V
–0.45 V
–0.50 V
–0.55 V
–0.60 V
e)
NGPC-900-5
J / mA cm-2
E / V vs. Ag/AgCl
100 rpm
400 rpm
900 rpm
1600 rpm
2500 rpm
f)
NGPC-900-5
J-1/ mA-1 cm2
f-1/2 / rpm-1/2
–0.25 V
–0.30 V
–0.35 V
–0.40 V
–0.60 V
g)
NGPC-1000-1
J / mA cm-2
E / V vs. Ag/AgCl
100 rpm
400 rpm
900 rpm
1600 rpm
2500 rpm
h)
NGPC-1000-1
J-1/ mA-1 cm2
f-1/2 / rpm-1/2
–0.25 V
–0.30 V
–0.35 V
–0.40 V
–0.60 V

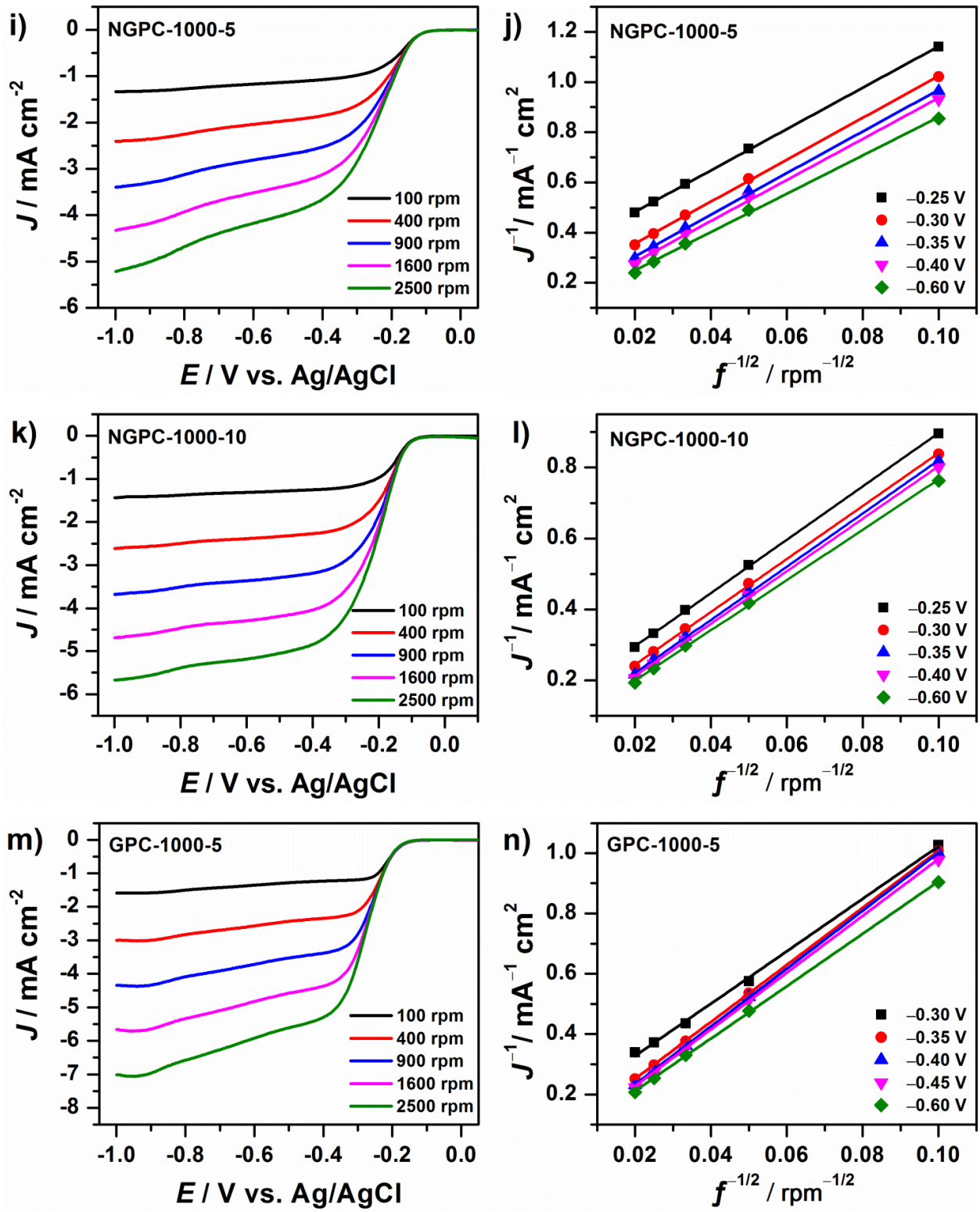
i)
NGPC-1000-5
J / mA cm-2
E / V vs. Ag/AgCl
100 rpm
400 rpm
900 rpm
1600 rpm
2500 rpm
j)
NGPC-1000-5
J-1 / mA-1 cm2
f-1/2 / rpm-1/2
–0.25 V
–0.30 V
–0.35 V
–0.40 V
–0.60 V
k)
NGPC-1000-10
J / mA cm-2
E / V vs. Ag/AgCl
100 rpm
400 rpm
900 rpm
1600 rpm
2500 rpm
l)
NGPC-1000-10
J-1 / mA-1 cm2
f-1/2 / rpm-1/2
–0.25 V
–0.30 V
–0.35 V
–0.40 V
–0.60 V
m)
GPC-1000-5
J / mA cm-2
E / V vs. Ag/AgCl
100 rpm
400 rpm
900 rpm
1600 rpm
2500 rpm
n)
GPC-1000-5
J-1 / mA-1 cm2
f-1/2 / rpm-1/2
–0.30 V
–0.35 V
–0.40 V
–0.45 V
–0.60 V

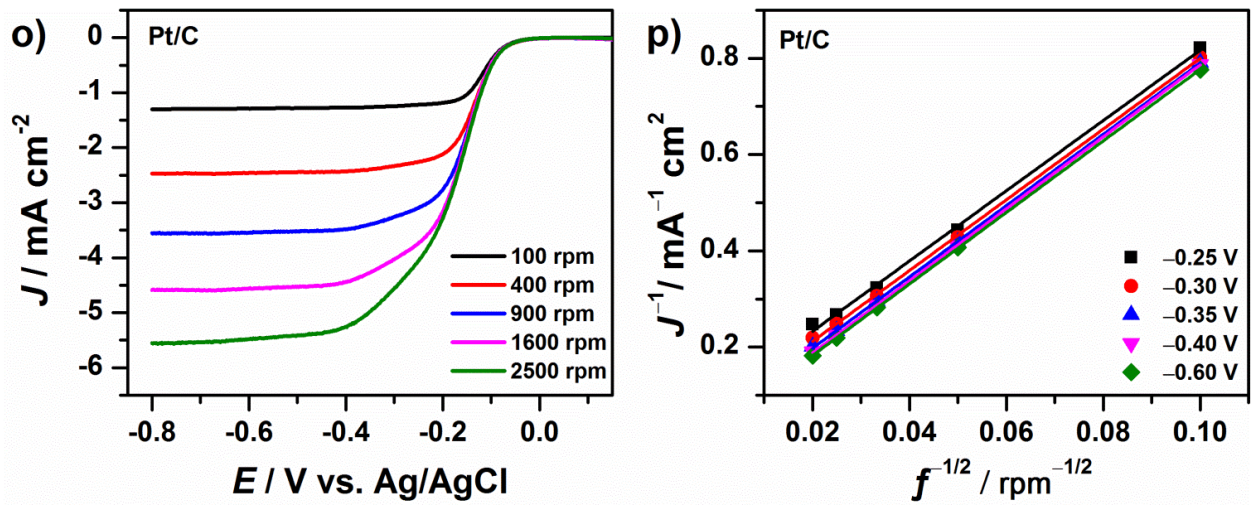

Fig. S16 LSV curves in O_2-saturated 0.1 M KOH solution with a sweep rate of 5 mV s^{-1} at different rotation rates and the corresponding K–L plots for different ORR catalysts. a, b) NGPC-700-5; c, d) NGPC-800-5; e, f) NGPC-900-5; g, h) NGPC-1000-1; i, j) NGPC-1000-5; k, l) NGPC-1000-10; m, n) GPC-1000-5 and o, p) 20 wt.% Pt/C.

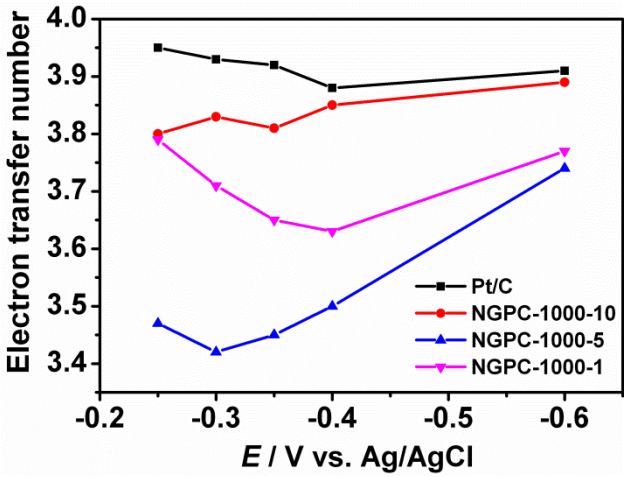

Fig. S17 Electron-transfer numbers as a function of the overpotential of NGPCs obtained at 1000 °C and commercial 20 wt.% Pt/C catalyst, respectively.

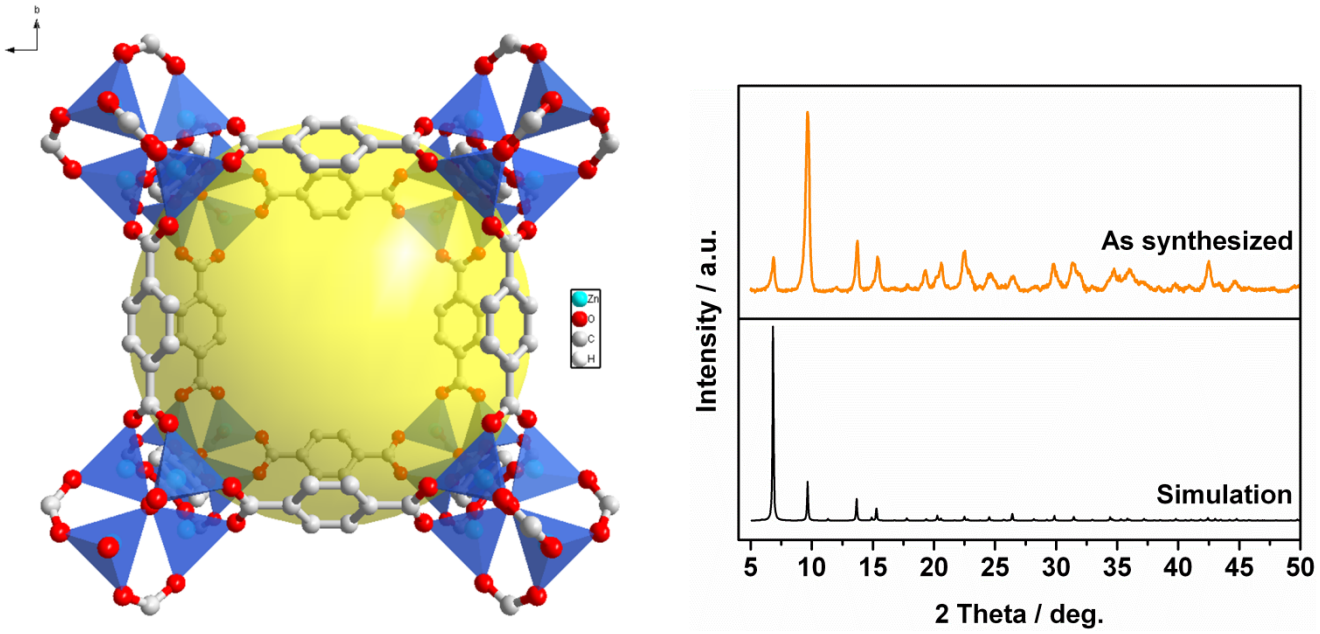

Fig. S18 Structural view (left) and powder X-ray diagram (right) of as-synthesized $[Zn_4O(bdc)_3]$ (MOF-5). Eight clusters (four visible) from an unit cell enclose a large cavity with diameter of 18.5 Å, indicated by a yellow sphere.

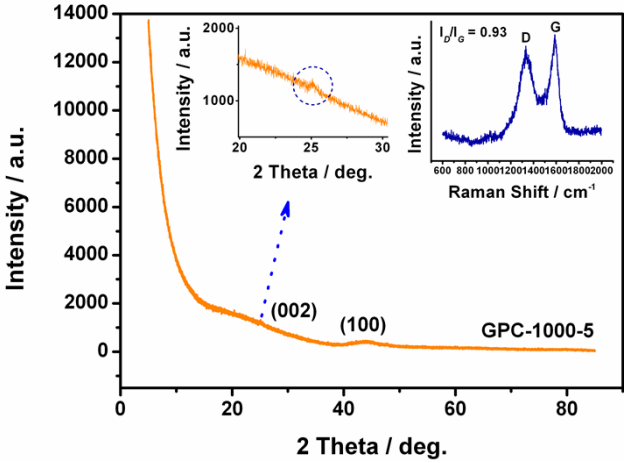

Fig. S19 PXRD diagram of MOF-5 derived carbon samples (GPC-1000-5); the insets are the enlargement of PXRD at position with 2θ value from 20° to 30° (left) and the corresponding Raman spectrum of the GPC-1000-5 (right).

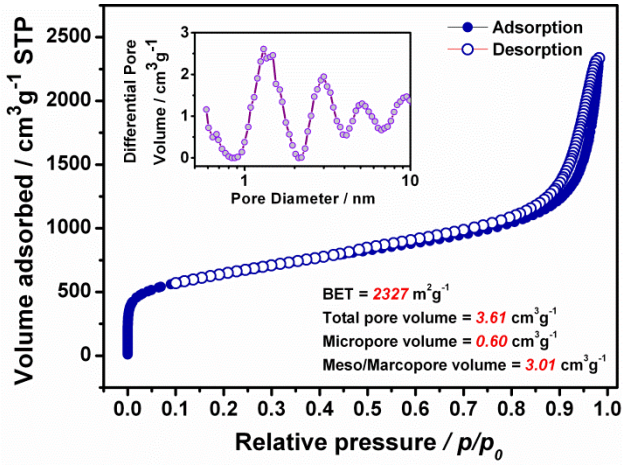

Fig. S20 Nitrogen sorption isotherms of MOF-5 derived carbon sample (GPC-1000-5) at 77 K, the inset gives the corresponding NL-DFT pore size distribution of the product.

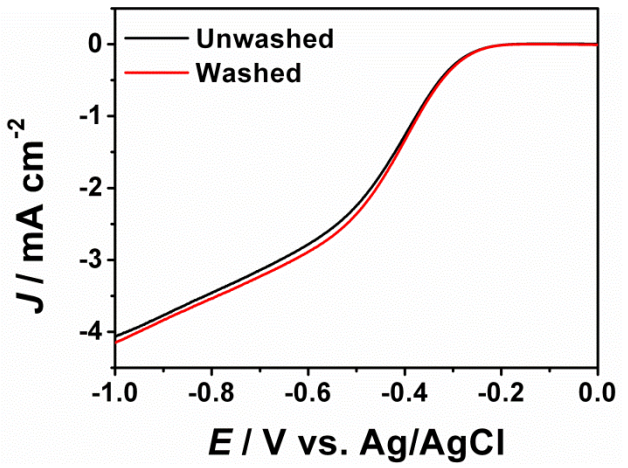

Fig. S21 Polarization curves of NGPC-800-5 with or without acid wash treatment. The results are obtained at conditions of 1600 rpm in an O_2-saturated 0.1 M KOH *aq*. solution at R.T., and a sweep rate of 5 mV s^{-1}.

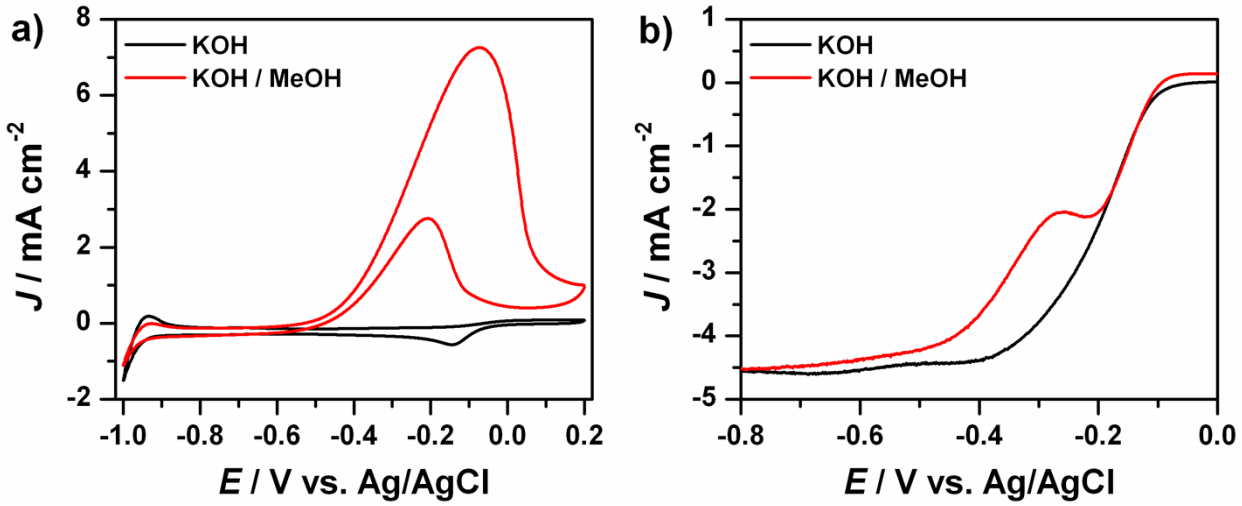

Fig. S22 a) CV and b) LSV curves of commercial Pt/C in O_2-saturated 0.1 M KOH solution with or without the addition of 3 M MeOH. The RDE measurements were carried out with a sweep rate of 5 mV s^{-1}, 1600 rpm.

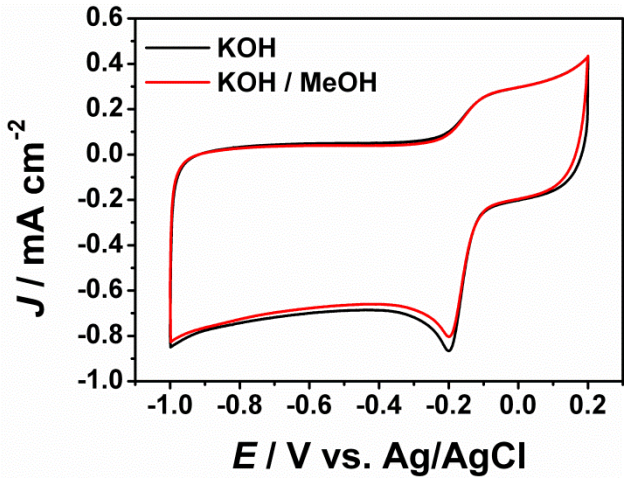

Fig. S23 CV curves of NGPC-1000-10 in O_2-saturated 0.1 M KOH solution at a scan rate of 10 mV s^{-1}, with or without the addition of 3 M methanol.

Table S2 Summary of ORR performance for some other nitrogen-doped metal-free catalysts and MOF-derived non-precious metal electrocatalysts (M/N/C) reported recently.

Heteroatom-doped carbon materials[a]	Synthetic methods (reaction precursors)	ORR performance *vs.* Pt/C[b]	Electron transfer number	Refs.
NGPC-1000-10	Nanaocasting of ZIF-8 nanocrystals	35 mV more negative in E_{onset}, comparable J_L of 4.67 mA cm^{-2} and J_K of 14.18 mA cm^{-2} at –0.35 V.	3.80–3.89 at range of –0.25 to –0.6 V	Present work
POF-C-1000	Nanocasting of PAF-6 and furfuryl alcohol	40 mV more negative in E_{onset}, 0.8 and 55 mA cm^{-2} less in J_L and J_K at –0.60 and –0.44 V *vs*. Hg/HgO	3.75 at –0.44 V *vs*. Hg/HgO	1
NCNFs	Carbonization of electrospun polyacrylonitrile nanofiber films	45 mV more negative in E_{onset}, *ca.* 1.0 mA cm^{-2} less in J_L	3.6–4.0 at range of –0.35 to –0.50 V	2
PN-ACNT	CVD with ferrocene,	80 mV more negative in E_{onset},	3.67–3.88	3

	pyridine and triphenylphosphine	higher cathodic current density below *ca.* –0.25 V *vs.*SCE	at –0.3 to –0.6 V *vs.*SCE	
N-S-G	Melamine, benzyl disulfide, graphene oxide with SiO_2 as template	30 mV more negative in E_{onset}, comparable J_L and nearly twice higher in J_K at –0.80 V	3.3–3.6 at most potential	[4]
NCNTs(BTA)	Carbonization of MWCNTs with Triazole and tetrazole derivatives	80 mV more negative in E_{onset}, comparable J_L at –0.9 V *vs.*SCE and 1.0 mA cm^{-2} higher in J_K at –0.5 V *vs.*SCE	3.62 at –0.5 V *vs.*SCE	[5]
N-HCNPs	CVD with trinitrophenol under high temperature and pressure	90 mV more negative in E_{onset}, comparable J_L at 1500 rpm and J_K at potential range of –0.3 to –0.4 V	3.70 at –0.4 V	[6]
CA-TCA_900	Hydrothermal carbonization with glucose/TCA	210 mV more negative in E_{onset}, comparable J_L at 1600 rpm	*ca.* 2.6–3.7 at range of –0.4 to –1.0 V	[7]
NG-1000	Direct annealing of graphene oxide/PDA	70 mV more negative in E_{onset}, comparable J_L at 1600 rpm and J_K at potential of –0.5 V *vs*. SCE	3.89 at –0.5 V *vs*. SCE	[8]
Acr@MW	Hydrothermally functionization of MWCNTs with aniline derivatives	38 mV more negative in E_{onset}, comparable J_L at 800 rpm	3.2 at –1.0 V	[9]
POMC-3	Nanocasting of SBA-15/triphenylphosphine	50 mV more negative in E_{onset}, comparable J_L at 1600 rpm	3.91 at –0.25 V	[10]
NG-NCNT	Hydrothermal treatment with Graphene oxide/oxidized MWCNTs/ammonia	70 mV more negative in E_{onset}, comparable J_L at 1600 rpm	3.3–3.7 at range of –0.4 to –0.7 V *vs*. SCE	[11]
NCNTs-20	Direct carbonization of Zn-Fe-ZIF/dicyandiamide	7 mV more positive in $E_{1/2}$, *ca.* 0.7 mA cm^{-2} higher in J_L at 1600 rpm	Not mentioned	[12]

[a] The samples listed in the table are the most efficient one chosen out from those reported in the corresponding literatures, respectively.

[b] All potentials are referred as Ag/AgCl scale, unless otherwise stated.

For comparison, all samples are tested in 0.1 M KOH solution under room temperature, unless otherwise stated.

The limiting current densities (J_L) are compared at a rotation speed of 1600 rpm, unless otherwise stated.

References

1. P. Pachfule, V. M. Dhavale, S. Kandambeth, S. Kurungot and R. Banerjee, *Chem.-Eur. J.*, 2013, **19**, 974-980.
2. D. Liu, X. Zhang, Z. Sun and T. You, *Nanoscale*, 2013, **5**, 9528-9531.
3. D. Yu, Y. Xue and L. Dai, *J. Phys. Chem. Lett.*, 2012, **3**, 2863-2870.
4. J. Liang, Y. Jiao, M. Jaroniec and S. Z. Qiao, *Angew. Chem., Int. Ed.*, 2012, **51**, 11496-11500.
5. A. Morozan, P. Jégou, M. Pinault, S. Campidelli, B. Jousselme and S. Palacin, *ChemSusChem*, 2012, **5**, 647-651.
6. G. Ma, R. Jia, J. Zhao, Z. Wang, C. Song, S. Jia and Z. Zhu, *J. Phys. Chem. C*, 2011, **115**, 25148-25154.
7. S.-A. Wohlgemuth, R. J. White, M.-G. Willinger, M.-M. Titirici and M. Antonietti, *Green Chem.*, 2012, **14**, 1515-1523.
8. H. P. Cong, P. Wang, M. Gong and S. H. Yu, *Nano Energy*, 2014, **3**, 55-63.

9. G. Tuci, C. Zafferoni, P. D'Ambrosio, S. Caporali, M. Ceppatelli, A. Rossin, T. Tsoufis, M. Innocenti and G. Giambastiani, *ACS Catal.*, 2013, **3**, 2108-2111.
10. D.-S. Yang, D. Bhattacharjya, S. Inamdar, J. Park and J.-S. Yu, *J. Am. Chem. Soc.*, 2012, **134**, 16127-16130.
11. P. Chen, T. Y. Xiao, Y. H. Qian, S. S. Li and S. H. Yu, *Adv. Mater.*, 2013, **25**, 3192-3196.
12. P. Su, H. Xiao, J. Zhao, Y. Yao, Z. Shao, C. Li and Q. Yang, *Chem. Sci.*, 2013, **4**, 2941-2946.